

Wave propagation in functionally graded materials by modified smoothed particle hydrodynamics (MSPH) method

G.M. Zhang ^{*}, R.C. Batra

*Department of Engineering Science and Mechanics, MC 0219, Virginia Polytechnic Institute and State University,
Blacksburg, VA 24061, United States*

Received 11 January 2006; received in revised form 14 June 2006; accepted 25 July 2006

Available online 11 September 2006

Abstract

We use the modified smoothed particle hydrodynamics (MSPH) method to study the propagation of elastic waves in functionally graded materials. An artificial viscosity is added to the hydrostatic pressure to control oscillations in the shock wave. Computed results agree well with the analytical solution of the problem. It is shown that, for the same placement of particles/nodes the MSPH method gives better results than the finite element method when the initial smoothing length in the MSPH method is 1.1 times the distance between two adjacent particles. Effects of the artificial viscosity are also examined, and the optimum value of the linear artificial viscosity that minimizes the relative error in computed stresses is found. © 2006 Elsevier Inc. All rights reserved.

Keywords: Functionally graded material; Meshless method; Wave propagation; Artificial viscosity

1. Introduction

Functionally graded structures are inhomogeneous bodies usually comprised of two constituents whose volume fractions vary continuously throughout the body so as to attain a specific variation of material moduli that minimizes a critical design variable, e.g. the maximum principal tensile stress or the maximum strain energy density, or the fundamental frequency of vibration. Lekhnitskii's [1] book has solutions to many linear elastic problems for inhomogeneous materials. Batra's [2] paper has an explicit solution and numerical results obtained by the finite element method (FEM) for the radial expansion of a circular Mooney–Rivlin cylinder with material moduli depending upon the radial coordinate. Interest in functionally graded materials (FGMs) seemed to originate with the International Symposium on FGMs [3]. Since the symposium, the literature on FGMs has exploded making a comprehensive review in the Section “Introduction” of a paper nearly impossible.

An advantage of FGMs is that the continuous variation of material properties eliminates sharp jumps in stresses that are likely to occur at interfaces between two distinct materials, as for example in laminated composites. This reduces the likelihood of two layers separating from each other. Also, under dynamic loading, there will be no wave reflections and refractions at such interfaces since material properties and the acoustic

^{*} Corresponding author. Tel.: +1 540 257 3966.

E-mail addresses: gazhang1@vt.edu (G.M. Zhang), rbatra@vt.edu (R.C. Batra).

impedance vary continuously; this reduces wave dispersions. However, in the traditional FEM, material properties are evaluated at Gauss or quadrature points, and stresses are generally discontinuous across interelement boundaries unless one uses a mixed formulation and takes stresses also as unknowns; e.g. see [4]. Of course, these additional unknowns increase the number of variables and hence the number of equations to be solved. Even when values of material properties at nodes are given as a part of the input data and values at quadrature points interpolated from these nodal values, stresses across interelement boundaries are discontinuous. Batra and Love [5] by using the traditional FEM to analyze transient plane strain deformations of a FG linear elastic body have shown that with a fine mesh the computed wave speed, wave profile and the axial stress at the wave front match very well with their values derived from the analytical solution of Chiu and Erdogan [6]. Here we use a meshless method, namely the modified smoothed particle hydrodynamics (MSPH) method [7], to study a plane strain elastodynamic problem and delineate the effect of various parameters on the accuracy of the computed solution.

The Lagrangian SPH method, due to Lucy [8] and Gingold and Monaghan [9], has been used by Libersky and Petschek [10] for analyzing finite deformations of an elastoplastic body. There are two weaknesses in the traditional SPH method: the boundary deficiency in the sense that basis functions do not satisfy consistency condition near the boundaries and the tensile instability. Chen et al. [11,12] proposed the corrective smoothed-particle method (CSPM) that removed the tensile instability deficiency of the SPH but not the boundary deficiency. However, the MSPH method is devoid of these two shortcomings of the SPH, and has been used to analyze two-dimensional transient heat conduction, wave propagation in a homogeneous linear elastic isotropic bar and the localization of deformation into a narrow zone of intense plastic deformation in thermoviscoplastic materials [13]. Sigalotti et al. [14] have proposed a technique to convert the standard SPH into a working shock capturing scheme without relying on solutions to the Riemann problem. Their modification allows solving problems with large discontinuities without using an artificial viscosity.

Wave propagation in FG elastic structures has numerically been studied by several investigators, e.g. see [15–18]; additional references may be found in [6]. Free and forced vibrations of FG plates by a meshless method have been analyzed, among others, in [19–26] and wave propagation in a segmented bar comprised of two materials by Batra and coworkers [27]. Here we study wave propagation, under uniaxial strain conditions, in a FG plate whose material properties vary continuously in the direction of wave propagation.

The rest of the paper is organized as follows. We review the MSPH method in Section 2, and formulate the wave propagation problem in an isotropic elastic body in Section 3. In Section 4 we compare the presently computed numerical solution with the analytical solution of Chiu and Erdogan [6], and delineate the effect on the accuracy of the computed solution of linear artificial viscosity, quadratic artificial viscosity, number of particles, smoothing length and the kernel function employed in the MSPH method. Findings of this work are summarized in Section 5 entitled conclusions.

2. The MSPH method

The Taylor series expansion of a function $f(\mathbf{x})$ about the point $\mathbf{x}^{(i)} = (x_1^{(i)}, x_2^{(i)}, x_3^{(i)})$ is

$$f(\xi) = f(\mathbf{x}^{(i)}) + \frac{\partial f}{\partial x_\alpha^{(i)}} (\xi_\alpha - x_\alpha^{(i)}) + \frac{1}{2} \frac{\partial^2 f}{\partial x_\alpha^{(i)} \partial x_\beta^{(i)}} (\xi_\alpha - x_\alpha^{(i)}) (\xi_\beta - x_\beta^{(i)}) + \cdots, \quad (2.1)$$

where a repeated index implies summation over the range of the index, an index enclosed in parentheses is not summed and Greek indices α, β and γ range over 1, 2 and 3. Multiplying both sides of Eq. (2.1) with a kernel function $W(\mathbf{x} - \xi, h)$ of compact support $2h$ (i.e., $W(\mathbf{x} - \xi, h) = 0$ for $|\mathbf{x} - \xi| \geq 2h$, $|\mathbf{x} - \xi|$ = distance between points \mathbf{x} and ξ), its first derivative $W_\gamma = \partial W / \partial \xi_\gamma$, its second derivative $W_{\gamma\delta} = \partial^2 W / \partial \xi_\gamma \partial \xi_\delta$, respectively, integrating over the domain Ω and neglecting the third and the higher derivative terms yield the following three equations:

$$\int_\Omega f(\xi) W d\xi = f_i \int_\Omega W d\xi + f_{xi} \int_\Omega (\xi_\alpha - x_\alpha^{(i)}) W d\xi + \frac{1}{2} f_{x\beta i} \int_\Omega (\xi_\alpha - x_\alpha^{(i)}) (\xi_\beta - x_\beta^{(i)}) W d\xi, \quad (2.2)$$

$$\int_\Omega f(\xi) W_\gamma d\xi = f_i \int_\Omega W_\gamma d\xi + f_{xi} \int_\Omega (\xi_\alpha - x_\alpha^{(i)}) W_\gamma d\xi + \frac{1}{2} f_{x\beta i} \int_\Omega (\xi_\alpha - x_\alpha^{(i)}) (\xi_\beta - x_\beta^{(i)}) W_\gamma d\xi, \quad (2.3)$$

$$\int_{\Omega} f(\xi) W_{\gamma\delta} d\xi = f_i \int_{\Omega} W_{\gamma\delta} d\xi + f_{\alpha i} \int_{\Omega} (\xi_{\alpha} - x_{\alpha}^{(i)}) W_{\gamma\delta} d\xi + \frac{1}{2} f_{\alpha\beta i} \int_{\Omega} (\xi_{\alpha} - x_{\alpha}^{(i)}) (\xi_{\beta} - x_{\beta}^{(i)}) W_{\gamma\delta} d\xi, \quad (2.4)$$

where $f_i = f(\mathbf{x}^{(i)})$, $f_{i,\alpha} = \partial f / \partial x_{\alpha}^{(i)}$, $f_{i,\alpha\beta} = \partial^2 f / \partial x_{\alpha}^{(i)} \partial x_{\beta}^{(i)}$ and $d\xi = d\xi_1 d\xi_2 d\xi_3$. Because the kernel function W is zero for $|\mathbf{x} - \xi| \geq 2h$ (h is the smoothing length), the integration domain Ω in Eqs. (2.2)–(2.4) equals the compact support of the kernel function. Eqs. (2.2)–(2.4) can be written in matrix form as

$$T = BF \quad \text{or} \quad T_I = B_{IJ} F_J, \quad I, J = 1, 2, \dots, 10, \quad (2.5)$$

where

$$\begin{aligned} B_{IJ} &= \int_{\Omega} \Phi(I) \Theta(J) d\xi = \sum_{j=1}^N \Phi(I) \Theta(J) \frac{m_j}{\rho_j}, \\ \Phi(1) &= W_{ij}, \quad \Phi(2) = W_{ij,x_1}, \quad \Phi(3) = W_{ij,x_2}, \quad \Phi(4) = W_{ij,x_3}, \\ \Phi(5) &= W_{ij,x_1x_1}, \quad \Phi(6) = W_{ij,x_2x_2}, \quad \Phi(7) = W_{ij,x_3x_3}, \\ \Phi(8) &= W_{ij,x_1x_2}, \quad \Phi(9) = W_{ij,x_2x_3}, \quad \Phi(10) = W_{ij,x_3x_1}; \\ \Theta(1) &= 1, \quad \Theta(2) = x_1^{(j)} - x_1^{(i)}, \quad \Theta(3) = x_2^{(j)} - x_2^{(i)}, \quad \Theta(4) = x_3^{(j)} - x_3^{(i)}, \\ \Theta(5) &= \frac{1}{2} (x_1^{(j)} - x_1^{(i)})^2, \quad \Theta(6) = \frac{1}{2} (x_2^{(j)} - x_2^{(i)})^2, \quad \Theta(7) = \frac{1}{2} (x_3^{(j)} - x_3^{(i)})^2, \\ \Theta(8) &= (x_1^{(j)} - x_1^{(i)}) (x_2^{(j)} - x_2^{(i)}), \quad \Theta(9) = (x_2^{(j)} - x_2^{(i)}) (x_3^{(j)} - x_3^{(i)}), \quad \Theta(10) = (x_1^{(j)} - x_1^{(i)}) (x_3^{(j)} - x_3^{(i)}); \\ F &= \{f_i, f_{i,x_1}, f_{i,x_2}, f_{i,x_3}, f_{i,x_1x_1}, f_{i,x_2x_2}, f_{i,x_3x_3}, f_{i,x_1x_2}, f_{i,x_2x_3}, f_{i,x_3x_1}\}^T, \\ T_I &= \int_{\Omega} f(\xi) \Phi(I) d\xi = \sum_{j=1}^N f_j \Phi(I) \frac{m_j}{\rho_j}, \quad W_{ij} = W(\mathbf{x}^{(i)} - \xi^{(j)}, h), \\ W_{ij,x_1} &= \left. \frac{\partial W}{\partial x_1} \right|_{\mathbf{x}=\mathbf{x}^{(i)}, \xi=\xi^{(j)}}, \quad W_{ij,x_1x_2} = \left. \frac{\partial^2 W}{\partial x_1 \partial x_2} \right|_{\mathbf{x}=\mathbf{x}^{(i)}, \xi=\xi^{(j)}}, \end{aligned} \quad (2.6)$$

m_j and ρ_j signify the mass and the mass density of the particle located at the point $\mathbf{x}^{(j)}$ and N denotes the number of particles in Ω . The smoothing length h determines a particle's support, the number N of other particles with which it interacts and is an important parameter that controls the accuracy of the solution. Eq. (2.5) is solved simultaneously for F_1, F_2, \dots, F_{10} .

Because the truncation error in Eq. (2.1) is of the order $|\xi - \mathbf{x}^{(i)}|^3$, the kernel estimate f_i , the first and the second derivatives $f_{\alpha i}$ and $f_{\alpha\beta i}$ obtained by solving Eq. (2.5) are second-order, first-order and zero-order consistent, respectively. In order for the matrix B in Eq. (2.5) to be nonsingular, N must equal at least 3, 6 and 10 for one-, two- and three-dimensional domain Ω , respectively.

A choice for the kernel function is the modified Gauss function

$$W(\mathbf{x} - \xi, h) = \begin{cases} \frac{G}{(h\sqrt{\pi})^{\lambda_d}} (e^{|\mathbf{x}-\xi|^2/h^2} - e^{-4}), & |\mathbf{x} - \xi| \leq 2h, \\ 0, & |\mathbf{x} - \xi| > 2h, \end{cases} \quad (2.7)$$

where λ_d represents the dimensionality of the space and the normalizing constant G equals 1.04823, 1.10081 and 1.18516 for $\lambda_d = 1, 2$ and 3, respectively. The modified Gauss function is continuous at $|\mathbf{x} - \xi| = 2h$, but its first- and second-order derivatives are discontinuous there.

3. Formulation of the problem

In rectangular Cartesian coordinates, the conservation equations of mass and linear momentum are

$$\frac{d\rho}{dt} = -\rho U_{,\beta}^{\beta}, \quad (3.1)$$

$$\frac{dU^{\alpha}}{dt} = \frac{1}{\rho} \sigma_{,\beta}^{\alpha\beta}, \quad (3.2)$$

where \mathbf{U} is the velocity vector, $\boldsymbol{\sigma}$ the Cauchy stress tensor and t the time. Here we study a mechanical problem, and do not consider the energy equation.

Writing the stress tensor as

$$\sigma^{\alpha\beta} = -P\delta^{\alpha\beta} + S^{\alpha\beta}, \quad (3.3)$$

we assume that the hydrostatic pressure P is proportional to the compression ratio. That is,

$$P = K \left(\frac{\rho}{\rho_0} - 1 \right), \quad (3.4)$$

where K is the bulk modulus and ρ_0 the initial mass density. The Jaumann rate of the deviatoric stress tensor \mathbf{S} is assumed to be related to the strain-rate tensor $\dot{\epsilon}^{\alpha\beta}$ by

$$\dot{S}^{\alpha\beta} - S^{\alpha\gamma} \dot{R}^{\beta\gamma} - S^{\gamma\beta} \dot{R}^{\alpha\gamma} = 2\mu \left(\dot{\epsilon}^{\alpha\beta} - \frac{1}{3} \delta^{\alpha\beta} \dot{\epsilon}^{\gamma\gamma} \right), \quad (3.5)$$

where μ is the shear modulus, δ the Kroneker delta and

$$\dot{\epsilon}^{\alpha\beta} = \frac{1}{2} \left(\frac{\partial U^\alpha}{\partial x^\beta} + \frac{\partial U^\beta}{\partial x^\alpha} \right), \quad (3.6)$$

$$\dot{R}^{\alpha\beta} = \frac{1}{2} \left(\frac{\partial U^\alpha}{\partial x^\beta} - \frac{\partial U^\beta}{\partial x^\alpha} \right). \quad (3.7)$$

Thus $\dot{\mathbf{R}}$ is the spin tensor. The smoothing length h is assumed to vary with deformations of the body, and is computed by solving

$$\frac{dh}{dt} = h U^\beta_{,\beta}. \quad (3.8)$$

As is rather well known, large oscillations occur near the shock wave. An artificial viscosity is usually introduced to diminish these oscillations and stabilize the numerical solution. The artificial viscosity Q , which includes both linear and quadratic terms in the volumetric strain rate $\dot{\epsilon}_v = \dot{\epsilon}^{\gamma\gamma}$, is defined as

$$Q = \begin{cases} -C_L \rho c \lambda \dot{\epsilon}_v + C_Q \rho \lambda^2 \dot{\epsilon}_v^2, & \dot{\epsilon}_v < 0, \\ 0, & \dot{\epsilon}_v \geq 0. \end{cases} \quad (3.9)$$

Here C_L and C_Q are, respectively, coefficients of the linear and the quadratic artificial viscosities, c is the sound speed, λ the characteristic length and $\dot{\epsilon}_v = U^\beta_{,\beta}$ the volumetric strain rate. Note that the positive artificial viscosity is introduced only when the volumetric strain rate is negative. The definition of λ is different for the MSPH and the FE methods; it equals the smoothing length h in the MSPH method, but the mesh size Δ in the FEM. Values of coefficients C_L and C_Q have significant influence on the computed solution; for the FEM, the usual values are 0.06 and 1.5 in LS-DYNA [28], while they are of order one in the SPH method. Monaghan [29] suggested their values near 1.0 and 2.0, respectively, while Libersky and Petschek [10] and Rabczuk et al. [30] set $C_L = C_Q = 2.5$. Johnson [31] used the SPH method to study wave propagation, and found that reasonable results were obtained for $C_L = 0.5$ and $C_Q = 1.0$. However, when their values were decreased to 0.05 and 1.0 respectively, large oscillations occurred near the shock wave. For $C_L = 0.2$ and $C_Q = 4.0$ oscillations were still present. Values of these coefficients, especially of the linear coefficient C_L , used in the SPH method are usually an order of magnitude larger than those used in the FEM.

With the artificial viscosity the stress tensor becomes

$$\sigma^{\alpha\beta} = -(P + Q)\delta^{\alpha\beta} + S^{\alpha\beta}. \quad (3.10)$$

In order to solve the problem numerically, Eqs. (3.1), (3.2), (3.5) and (3.8) are assumed to hold at each particle. Kernel estimates of $U^\beta_{,\gamma}$ and $\sigma^{\alpha\beta}_{,\gamma}$, computed from Eq. (2.5), are substituted into these equations. The resulting coupled linear ordinary differential equations are integrated with respect to time t by the central-difference method.

The stable time step δt_i of particle i is determined by the Courant–Friedrich–Lewy condition:

$$\delta t_i = 0.3 \frac{h_i}{c_i + |\mathbf{U}_i|}, \quad (3.11)$$

where c_i is the sound speed at particle i , h_i its smoothing length and $|\mathbf{U}_i|$ its speed. We choose the time step $\Delta t = \min\{\delta t_i, i = 1, 2, \dots, N_{\text{tot}}\}$, where N_{tot} equals the total number of particles.

Here we study a uniaxial strain problem, namely that of wave propagation in an isotropic and inhomogeneous plate because an analytical solution of the problem is available; a schematic sketch of the problem studied is shown in Fig. 1. We set all components except $\dot{\epsilon}_{yy}$ of the strain-rate tensor equal to zero and tacitly assume that the plate dimensions in x - and z -directions are very large as compared to l . Young's modulus, E , and the mass density, ρ , are assumed to vary in the y -direction according to the relations

$$E(y) = E_0 \left(1 + a \frac{y}{l}\right)^m, \quad (3.12)$$

$$\rho(y) = \rho_0 \left(1 + a \frac{y}{l}\right)^n, \quad (3.13)$$

where l is the length of the body in the y -direction, a , m and n are material constants, E_0 and ρ_0 are Young's modulus and the mass density at $y = 0$. From Young's modulus, E , and Poisson's ratio, ν , one can compute the bulk modulus, K and the shear modulus, μ , from

$$K = \frac{E}{3(1 - 2\nu)}, \quad (3.14)$$

$$\mu = \frac{E}{2(1 + \nu)}. \quad (3.15)$$

As in the analytical solution of Chiu and Erdogan [6], the Poisson ratio is taken to be a constant throughout the body.

An impulsive load given by

$$\sigma(l, t) = \sigma_0 [H(t) - H(t - t_0)] \quad (3.16)$$

is applied on the right edge $y = l$ of the plate. Here H is the Heaviside step function. The left face of the plate is traction free; i.e.,

$$\sigma(0, t) = 0. \quad (3.17)$$

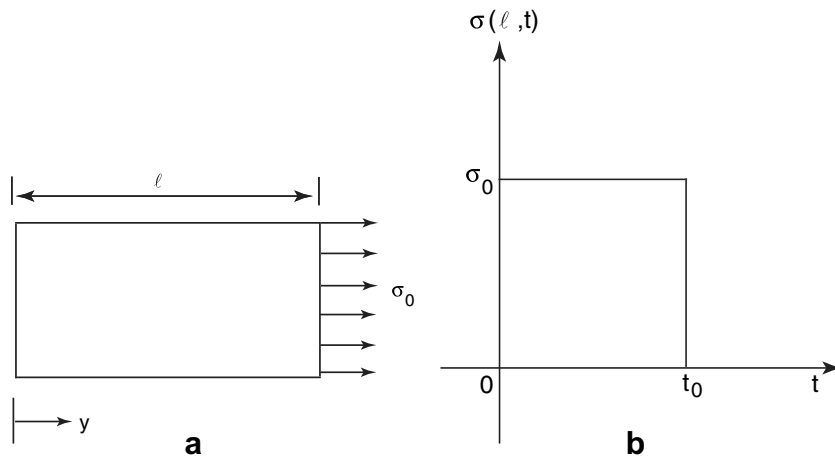


Fig. 1. (a) An inhomogeneous elastic plate free at the left end and loaded by an axial traction applied at the right end; (b) axial traction at the right end vs. time, t .

4. Numerical results

Values of various parameters used to compute results are

$$\begin{aligned} E_0 &= 226.9 \text{ GPa}, \quad \nu = 0.33, \quad \rho_0 = 8900 \text{ kg/m}^3, \\ a &= 0.3, \quad m = 3, \quad n = 1, \quad l = 5 \text{ mm}, \quad C_L = 0.2, \quad C_Q = 4.0, \\ \sigma_0 &= 1.0 \text{ GPa}, \quad t_0 = 3 \mu\text{s}. \end{aligned}$$

Five hundred uniformly distributed particles are located along the length of the plate in the y -direction, and the initial smoothing length, h , is set equal to 1.1Δ where Δ is the distance between two adjacent particles.

Fig. 2(a)–(d) compares at four different times, $2 \mu\text{s}$, $4 \mu\text{s}$, $7.11 \mu\text{s}$ and $12 \mu\text{s}$, the distribution of the axial stress σ with that obtained from the analytical solution of Chiu and Erdogan [6]. Subsequent to the application of the load on the right face, an elastic wave propagates towards the left end. Due to the spatial variation of E and ν , the elastic wave speed C_e is not constant; it is given by

$$C_e = \sqrt{\frac{(1-\nu)}{(1+\nu)(1-2\nu)} \frac{E}{\rho}} = \sqrt{\frac{E_0}{\rho_0} \left(a \frac{y}{l} + 1\right)^{\frac{m-n}{2}}} = \sqrt{\frac{E_0}{\rho_0} \left(a \frac{y}{l} + 1\right)}. \quad (4.1)$$

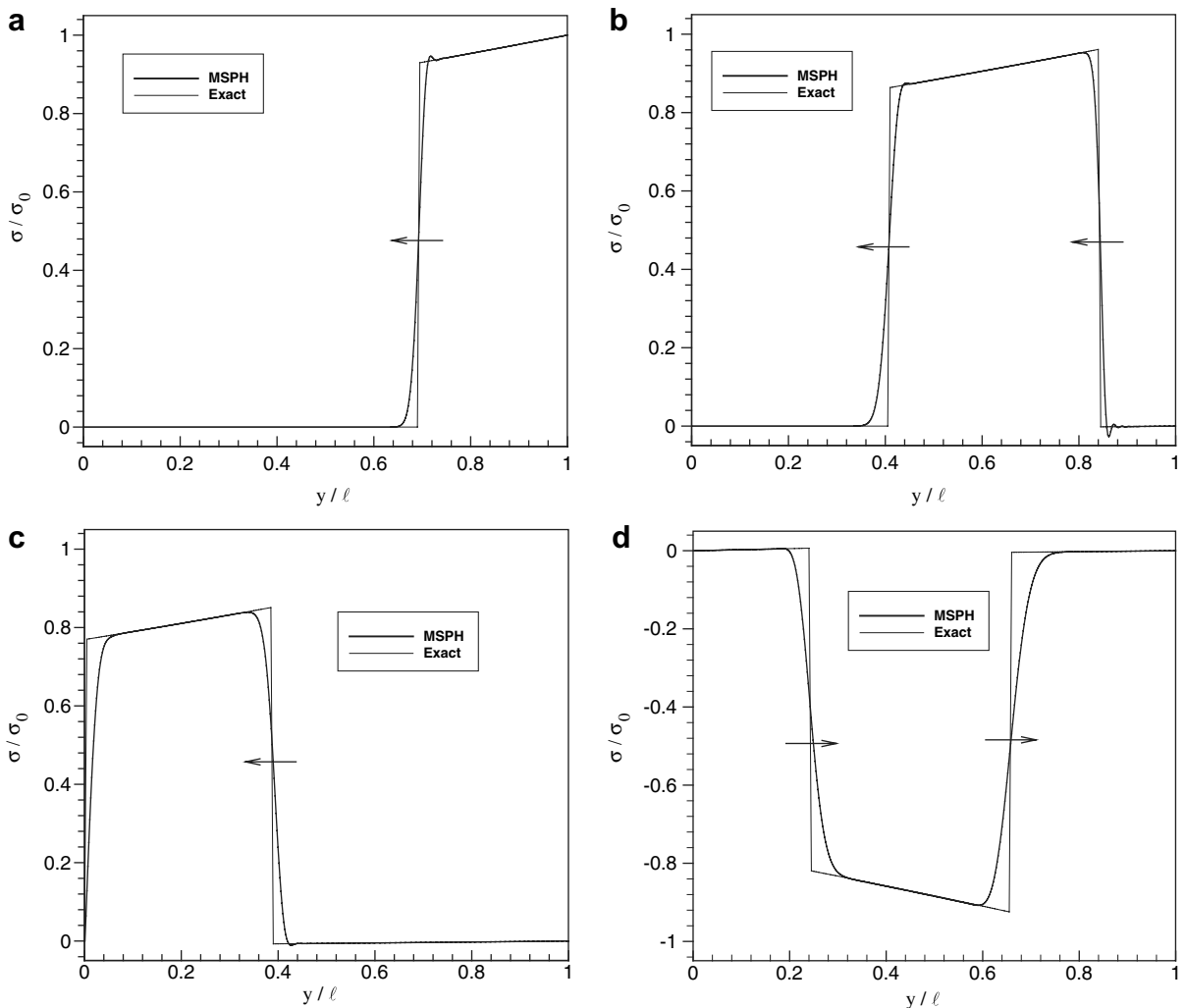


Fig. 2. Comparison of the distribution of the axial stress σ in the plate computed by the MSPH method with that obtained from the analytical solution at time (a) $2 \mu\text{s}$, (b) $4 \mu\text{s}$, (c) $7.11 \mu\text{s}$ and (d) $12 \mu\text{s}$.

The wave speed varies affinely in the y -direction. It takes $T = \int_0^l \frac{1}{C_e} dy = 7.11423 \mu\text{s}$ for the wave to traverse the plate. For $t > 3 \mu\text{s}$, the applied load becomes zero and an elastic unloading wave propagates from the right to the left edge with the wave speed C_e given by Eq. (4.1); see Fig. 2(b).

From Eq. (41) of [6], the magnitude of the jump discontinuity in the axial stress σ across the wave front is given by

$$\frac{\Delta\sigma}{\sigma_0} = \left[\frac{ay/l + 1}{a + 1} \right]^{\frac{m+n}{4}}. \quad (4.2)$$

It is clear that for $m + n > 0$, the magnitude of the stress wave will decrease from $y = l$ to $y = 0$.

We note that the acoustic impedance, $D(y)$, of the material is given by

$$D(y) = \rho C_e = \sqrt{E_0 \rho_0} \left(a \frac{y}{l} + 1 \right)^{\frac{m+n}{2}}. \quad (4.3)$$

Substitution from Eq. (4.3) into Eq. (4.2) gives

$$\frac{\Delta\sigma}{\sigma_0} = \sqrt{\frac{D(y)}{D(l)}}. \quad (4.4)$$

Thus the acoustic impedance determines the variation of the magnitude of the axial stress σ . For constant acoustic impedance, $\Delta\sigma = \sigma_0$. For example, for a homogeneous material, $m = n = 0$ and $\Delta\sigma = \sigma_0$. In the present problem, $m + n = 4$, $\frac{\Delta\sigma}{\sigma_0} = \frac{ay/l+1}{a+1}$ and the magnitude of stress wave varies affinely with y as it propagates from right to left in the plate. When the stress wave reaches the left end face (see Fig. 2(c)), its magnitude is given by

$$\sigma(0) = \frac{0+1}{a+1} \sigma_0 = 0.76923 \sigma_0.$$

From the left end, it is reflected as a negative stress wave, see Fig. 2(d).

It can be seen from Fig. 2 that computed positions of the wave front coincide with those given by the exact solution. The magnitudes of the computed axial stress at different times also agree well with those given by the exact solution except near the wave front. The wave front is distorted due to the dissipation introduced by the artificial viscosity. In Section 4.2 we use results at $4 \mu\text{s}$ to examine the effect of the artificial viscosity.

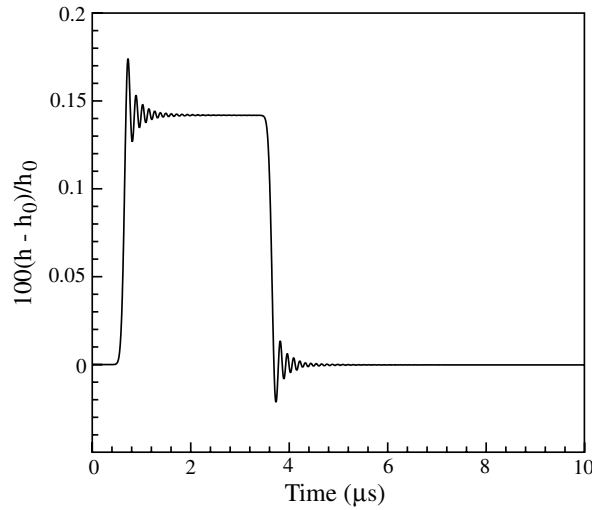
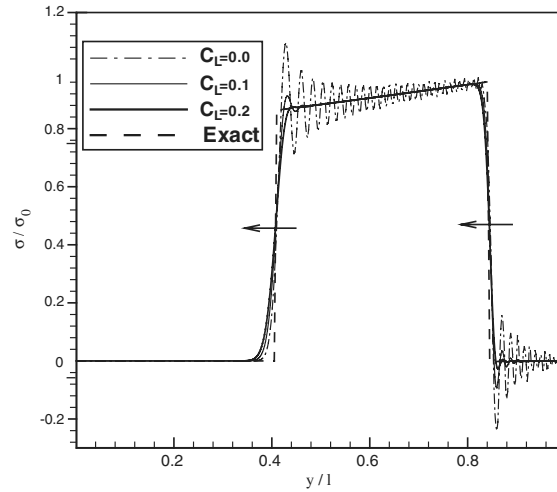
4.1. Variation with time of the smoothing length

Fig. 3 depicts the time history of the change in the smoothing length at the particle located at $y/l = 0.9$. It shows that the smoothing length changes by less than 0.2% during the passage of the elastic wave at this point; a similar variation of h with time is observed at other particles. Thus for the present problem, we keep the smoothing length unchanged.

4.2. The effect of the linear artificial viscosity

We first study the effect of the linear artificial viscosity and set the coefficient C_Q equal to zero. Fig. 4 exhibits the stress profile, at $4 \mu\text{s}$, computed with three different values, 0.0, 0.1 and 0.2, of C_L . It can be seen that in the absence of artificial viscosity, the solution oscillates, the amplitude of oscillations is maximum near the wave front, and oscillations decay in the wake of the wave. The largest amplitude of the stress wave is about 20% more than that given by the exact solution. With an increase in the value of C_L , oscillations decrease and disappear gradually. However, the wave front becomes less sharp for larger values of C_L . For good quality computed results, these oscillations should be small or absent and the wave front be steep. Thus it is difficult to determine the optimum value of the linear artificial viscosity without introducing a scalar measure of the error in the computed stress profile.

Accordingly, we introduce the following relative error in the axial stress to ascertain the accuracy of the computed solution:

Fig. 3. Time history of $100(h - h_0)/h_0$.Fig. 4. At $t = 4 \mu\text{s}$, variation of the axial stress in the plate for different values of C_L .

$$\eta = \frac{\int_0^l |\sigma - \sigma^{\text{exact}}| dy}{\int_0^l |\sigma^{\text{exact}}| dy}. \quad (4.5)$$

The relative error η computed with different values of the artificial viscosity coefficient is depicted in Fig. 5 for 150, 300, 500 and 1000 uniformly spaced particles. In order to compare results from the MSPH method with those from the FEM we have included results from the FEM computed with nodes coincident with particles of the MSPH method. Because the smoothing length h plays an important role in the MSPH method, we have also computed results with three other values 1.5Δ , 2.0Δ and 2.5Δ , of the initial smoothing length.

It is obvious that these results can be divided into three stages. In the first stage, an increase in C_L decreases the amplitude of oscillations. In this stage η decreases rapidly with an increase in C_L , the amplitude of oscillations decreases that lowers η but the wave front becomes less sharp that increases η . With a further increase in the value of C_L , the two effects are of the same order of magnitude, the relative error η in the axial stress σ changes slowly, which can be regarded as a relatively flat phase. We define the optimum value of the artificial viscosity as being one which minimizes η , and set it equal to y_c . With a further increase in the value of the coefficient of linear artificial viscosity, for example when it is greater than 0.2, η has a larger contribution from

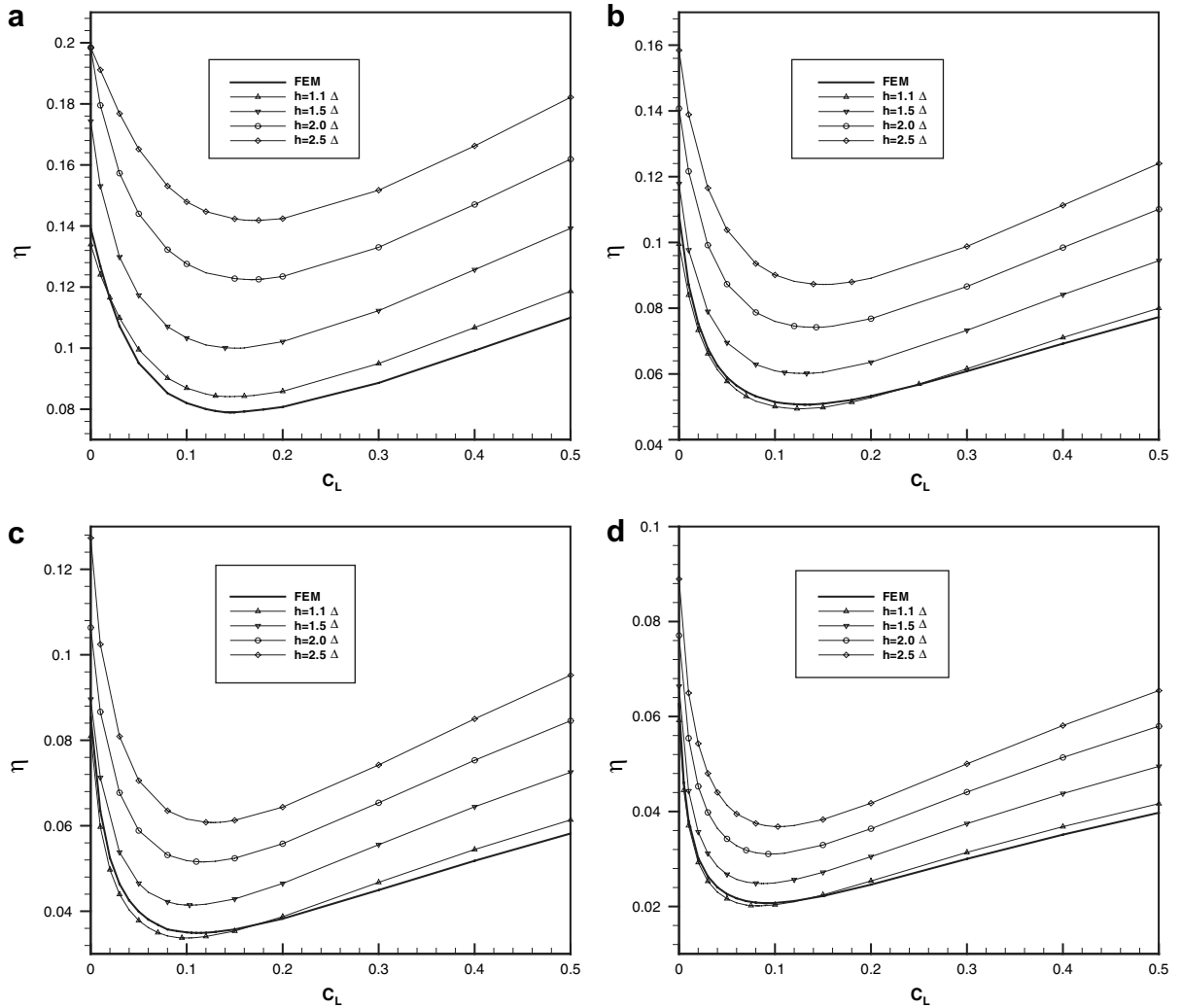


Fig. 5. At time $t = 4 \mu\text{s}$, variation of the relative error in the axial stress σ with the linear artificial viscosity coefficient for (a) 150, (b) 300, (c) 500 and (d) 1000, particles computed with (i) the MSPH method by using different values of the initial smoothing length and (ii) the FEM by using the same nodal locations as in the MSPH method.

the shape of the wave front than that from oscillations in the stress profile. In this stage, oscillations essentially disappear; see Fig. 4.

It is clear that the linear artificial viscosity plays an important role in the error in the relative stress. Let η_{\min} denote the minimal value of the error in the relative stress, and η_0 the error in the relative stress when $C_L = 0.0$. The ratio η_{\min}/η_0 for the FE and the MSPH methods with $h = 1.1\Delta$ and different number of particles/nodes is compared in Table 1. Thus an appropriate value of the linear artificial viscosity can greatly reduce the error in the relative stress and improve the results. Also with the increase in the number of particles, the improvement is enhanced. For small number of particles/nodes, the FEM gives a lower value of the relative error than the MSPH method. However, for the number of particles equal to or greater than 500, the two methods have virtually the same value of η_{\min}/η_0 .

One can conclude from results depicted in Fig. 5, that the error η increases with a decrease in the number of particles for both the FE and the MSPH methods. For the MSPH method, η increases with an increase in the smoothing length. The influence of the smoothing length upon η will be further explored in Section 4.6.

From the plots of Fig. 5 we conclude that for $h = 1.1\Delta$, errors η in results computed by the MSPH and the FE methods are nearly the same. It can also be seen that the MSPH method with $h = 1.1\Delta$ will give better

Table 1

Comparison of the ratio η_{\min}/η_0 between the FE and the MSPH methods with $h = 1.1\Delta$

Number of particles	150	300	500	1000
FE	0.567	0.468	0.409	0.331
MSPH	0.628	0.497	0.417	0.340

results than the FEM for $C_L \leq 0.02, 0.24, 0.18$ and 0.14 for 150, 300, 500 and 1000 particles, respectively. We note that in the initial phase, the slope of curves in Fig. 5 computed by the MSPH method with $h = 1.1\Delta$ is greater than that of curves obtained with the FEM. This is because the characteristic length $\hat{\lambda}$ for the MSPH method is 1.1Δ , but that for the FEM is Δ . In order to compare effects of the artificial viscosity on results computed with the FE and the MSPH methods, the abscissa must be replaced by the equivalent linear artificial viscosity coefficient $C_L\hat{\lambda}/\Delta$, as has been done in Fig. 6. For 300, 500 and 1000 particles, the relative error η in the axial stress computed with the MSPH method is smaller than that with the FEM for all values of the linear artificial viscosity coefficient. But when the number of particles decreases, the relative error η of the MSPH solution increases a little faster than that of the FE solution. For example, when the number of

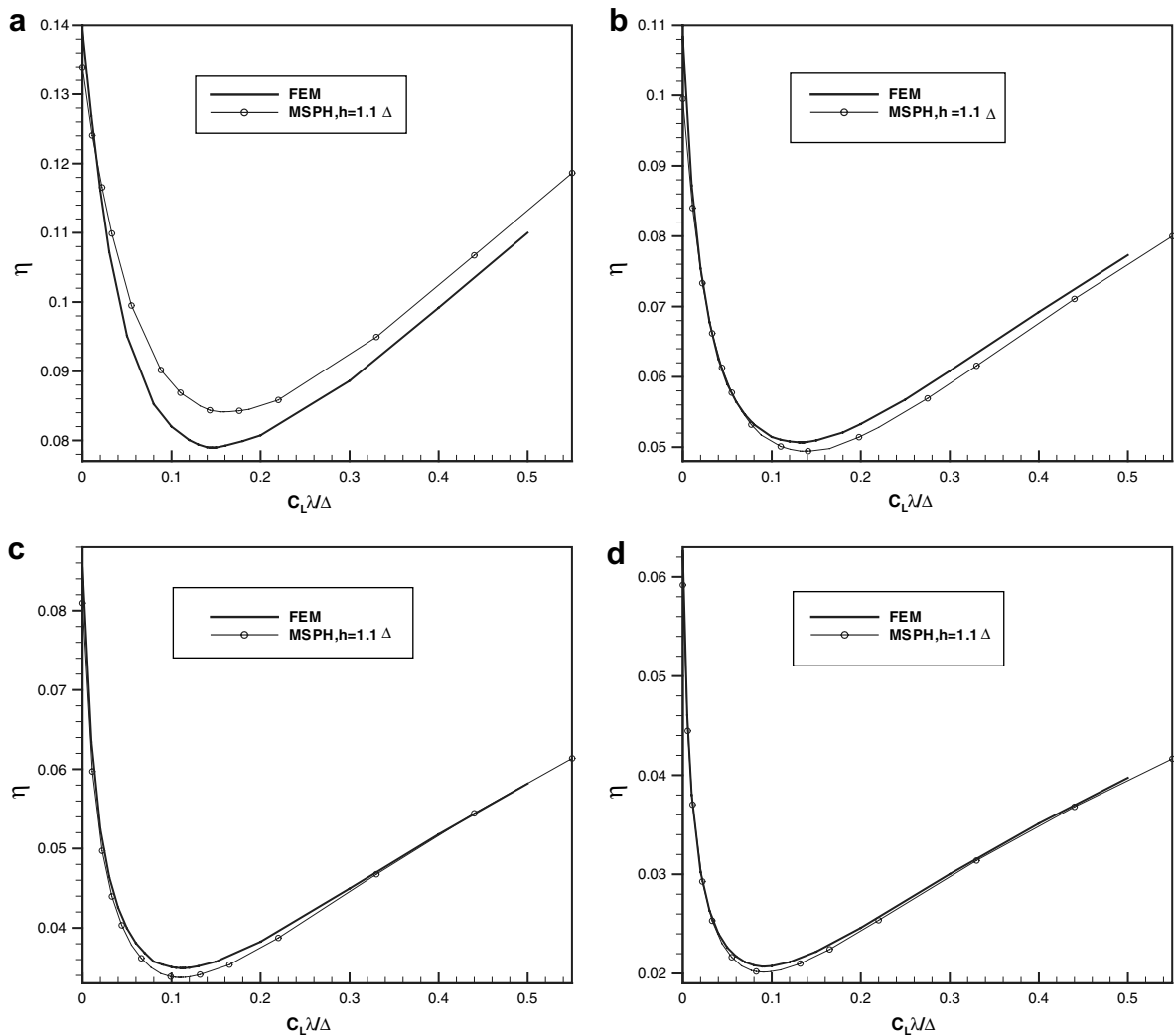


Fig. 6. At time = $4 \mu\text{s}$, variation of the relative stress error η with the equivalent coefficient of the linear artificial viscosity for (a) 150, (b) 300, (c) 500 and (d) 1000, particles computed by the MSPH and the FE methods.

particles is 150, the relative error of the MSPH method is greater than that of the FEM, except when C_L is very small; cf. Fig. 6(a).

Table 2 gives values of the equivalent linear artificial viscosity coefficient for the MSPH method with $h = 1.1\Delta$ and the FEM. It is obvious that the two values of the equivalent linear artificial viscosity are nearly the same, except when the number of particles is small, for example, 150.

4.3. Optimum value of linear artificial viscosity

Since the linear artificial viscosity coefficient noticeably affects results, it is important to determine the value of the coefficient C_L that gives “best” results. Ideally, this value of C_L should not depend on the smoothing length h and the number of particles. Recall that y_c equals the value of C_L that minimizes η . In Table 3, we list y_c for different values of h , and for different number of particles. For a fixed number of particles y_c increases with an increase in the smoothing length h . However, for a fixed h y_c decreases with an increase in the number of particles.

Fig. 7 shows the variation in y_c with the dimensionless particle distance Δ/l for the MSPH method with $h = 1.1\Delta$. It is clear that y_c decreases with a decrease in Δ/l , the curve y_c vs. Δ/l is not smooth, and the range of y_c is rather large. Fig. 8(a) compares the relative stress error computed with y_c (indicated by the solid line)

Table 2
For different number of particles, comparison of the equivalent linear artificial viscosity between the FE and the MSPH methods with $h = 1.1\Delta$

	150	300	500	1000
FE	0.148	0.135	0.112	0.091
MSPH, $h = 1.1\Delta$	0.156	0.136	0.110	0.090

Table 3
Values of y_c for different smoothing lengths and number of uniformly spaced particles

Number of particles\h	1.1Δ	1.5Δ	2.0Δ	2.5Δ
150	0.142	0.154	0.168	0.170
300	0.124	0.132	0.142	0.151
500	0.100	0.103	0.116	0.127
1000	0.082	0.087	0.095	0.103

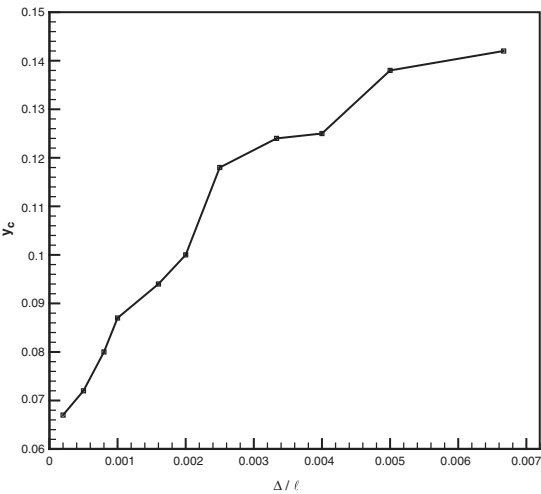


Fig. 7. Variation of y_c with the dimensionless distance between two adjacent particles.

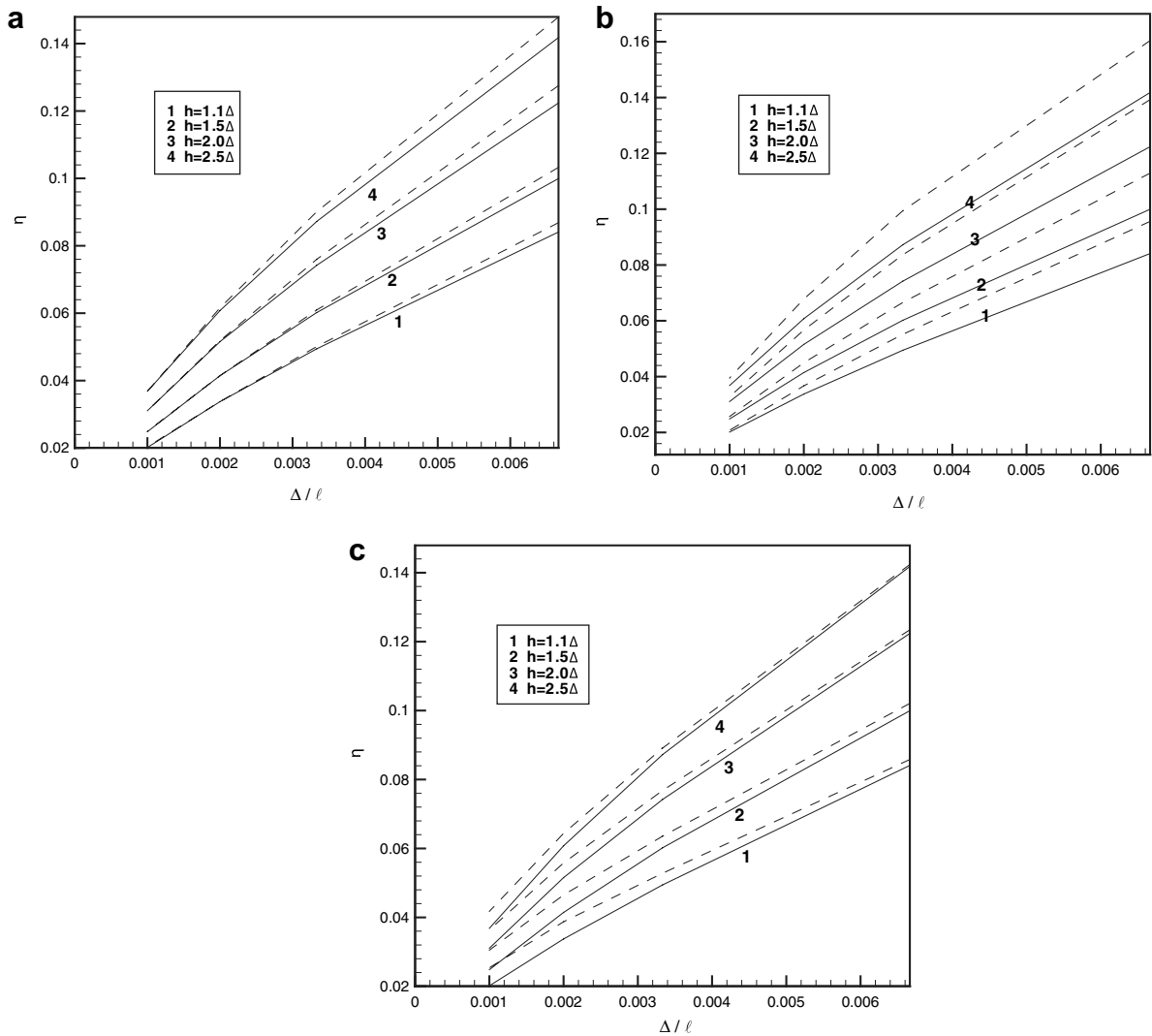


Fig. 8. For $h = 1.1\Delta$, 1.5Δ , 2.0Δ and 2.5Δ , comparison of the relative stress error η vs. Δ/l for η computed with $C_L = y_c$ (solid curve) and that (dashed curve) with (a) $C_L = 0.1$, (b) $C_L = 0.06$ and (c) $C_L = 0.2$.

with that for $C_L = 0.1$ (indicated by the dash line) for different smoothing lengths; the difference between the two diminishes with a decrease in the dimensionless particle distance Δ/l , and for $\Delta/l = 0.001$, the two curves coincide with each other. The results computed with $C_L = 0.06$ and y_c and $C_L = 0.2$ and y_c are compared in Fig. 8(b) and (c). When $C_L = 0.06$, the value used in the FEM, the difference between η for $C_L = 0.06$ and that for $C_L = y_c$ is much bigger although it decreases when Δ/l decreases. For $C_L = 0.2$, and $C_L = y_c$ the difference between the two sets of results increases when Δ/l decreases, and results do not converge to the analytical solution. If C_L is taken equal to the value often used in the SPH method, for example, 0.5, 1.0 or 2.5, from Fig. 5 it can be seen that the relative stress error will be much larger. So 0.1 is a better value for C_L in the MSPH method to simulate wave propagation in the FG plate. This value is larger than the 0.06 often used in the FEM, and is much smaller than that used in the SPH method.

4.4. Effect of quadratic artificial viscosity

With the linear artificial viscosity coefficient C_L set equal to zero, Fig. 9 shows the variation of the relative stress error η with the quadratic artificial viscosity coefficient C_Q . It is found that C_Q has negligible effect on

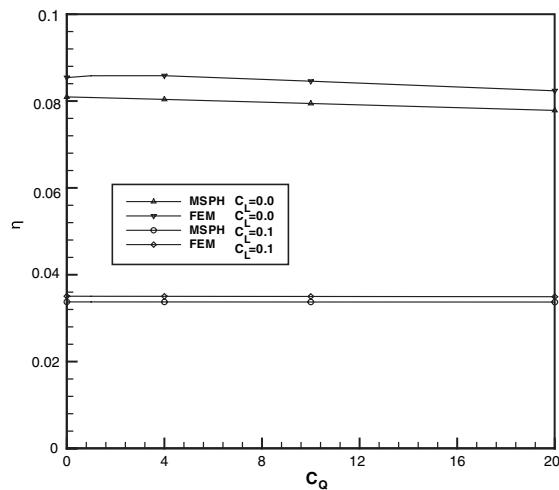


Fig. 9. Variation of the relative stress error η with C_Q for the FEM and the MSPH method with $h = 1.1\Delta$.

results. For the MSPH method with $h = 1.1\Delta$, η decreases from 0.081 to 0.078 when C_Q is increased from 0 to the rather large value, 20. If the linear artificial viscosity is included, the effect of quadratic artificial viscosity is even smaller, and η only decreases by about 0.1% when C_Q is increased from 0 to 20.

Since the effect of the quadratic artificial viscosity is negligible, it has been ignored while computing results presented below.

4.5. Effect of the number of particles

For uniformly spaced particles and $h = 1.1\Delta$ Fig. 10 exhibits the variation of η with Δ/l for the MSPH and the FE methods; nodes in the FE method coincide with particles in the MSPH method. C_L in the MSPH method is taken equal to 0.1, while C_L equals 0.11 in the FEM so as to have the same value of the equivalent linear artificial viscosity coefficient in the two methods. Note that the number of particles equals l/Δ . For both methods the relative stress error changes nearly linearly with Δ/l . The relative stress error for the MSPH

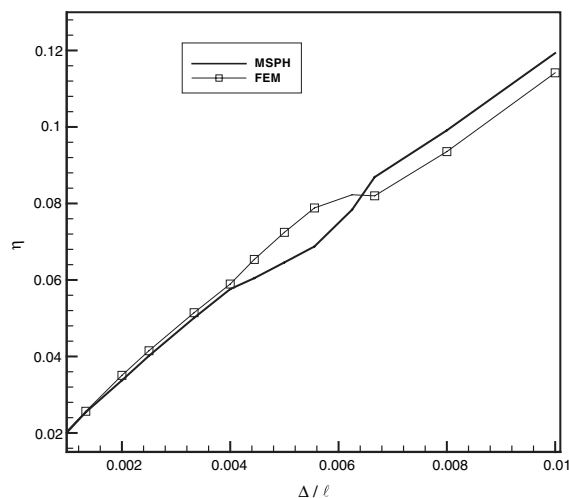


Fig. 10. Variation of the relative stress error η with the dimensionless distance between adjacent particles for the MSPH with $h = 1.1\Delta$ and the FEM.

method is a little smaller than that for the FEM when Δ/l is less than 0.0066, but the reverse holds for $\Delta/l > 0.0066$.

4.6. Effect of the smoothing length h

For 500 particles and $C_L = 0.1$, Fig. 11 shows the variation of the relative stress error with h/Δ . The relative stress error increases linearly with the increase in the smoothing length; so a smaller smoothing length will give better results. However, as stated in Section 2, the smoothing length must be such that the matrix B is non-singular. In a one-dimensional problem, for every particle to have at least two other particles in its support, the smoothing length must be greater than Δ ; otherwise the compact support of the kernel of a boundary particle will contain two particles and the matrix B will be singular. This value of the smoothing length depends on the maximum strains that occur in the problem. For the problem studied, $h = 1.1\Delta$ is sufficient to ensure the invertibility of the matrix B . But in problems involving large deformations, the smoothing length will vary with deformations, and the initial smoothing length should have a larger value.

4.7. Effect of the kernel function

Another important parameter in the MSPH method is the kernel function; three often-used kernel functions are listed below.

Gauss function:

$$W(d, h) = \frac{1}{(h\sqrt{\pi})^{1/d}} e^{-d^2};$$

Quartic spline function:

$$W(d, h) = \frac{G}{h^{1/d}} \begin{cases} 1 - \frac{3}{2}d^2 + d^3 - \frac{3}{16}d^4, & 0 \leq d \leq 2, \\ 0 & 2 < d; \end{cases}$$

Cubic B-spline function:

$$W(d, h) = \frac{G}{h^{1/d}} \begin{cases} 1 - \frac{3}{2}d^2 + \frac{3}{4}d^3 & 0 \leq d < 1, \\ [2 - d]^3 & 1 \leq d \leq 2, \\ 0 & 2 < d; \end{cases}$$

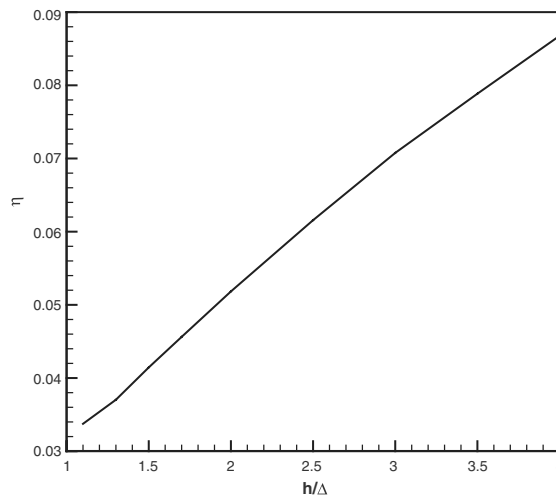


Fig. 11. Variation of the relative stress error η with the dimensionless smoothing length, h/Δ .

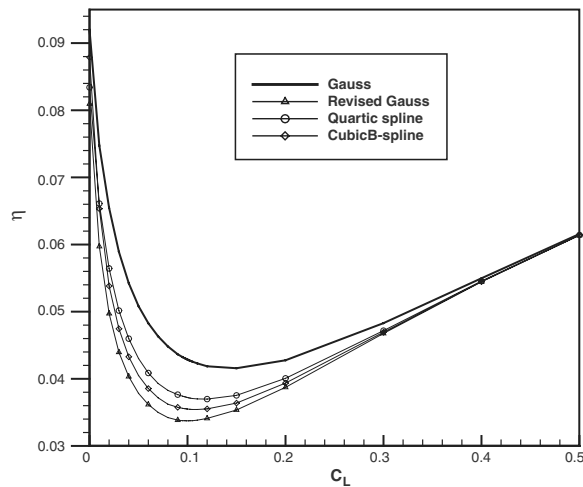


Fig. 12. Variation of the relative stress error η with C_L for four different kernel functions.

where $d = |\mathbf{x} - \xi|/h$, and λ_d equals the dimensionality of the space. For $\lambda_d = 1, 2$ and 3 , $G = 5/8, 5/4\pi$ and $105/128\pi$ for the quartic spline function, and $G = 2/3, 10/7\pi$ and $1/\pi$ for the cubic B-spline function.

For 500 particles, and $h = 1.1\Delta$, Fig. 12 depicts the variation with the linear artificial viscosity coefficient of the relative stress error computed with these three kernel functions and the modified Gauss function (2.7). It is clear that the modified Gauss kernel function gives the smallest value of η regardless of the value of the linear artificial viscosity coefficient, while the Gauss kernel function has the largest value of η . The difference in the values of η decreases with an increase in the value of the linear artificial viscosity coefficient, and it vanishes for large values of C_L . The maximum difference between results with the Gauss function and the modified Gauss function is about 1%, which is large when compared to η_{\min} of 3.4%. It seems that the modified Gauss function is a good choice for the kernel function in the MSPH method.

4.8. Remarks

We have found optimum values of the smoothing length, coefficient of linear artificial viscosity, the kernel function and the number of particles for one spatial variation of material parameters along the plate length. Finding the optimum set of values for different combinations of values of m, n and a in Eqs. (3.12) and (3.13) is an arduous task, and has not been attempted here. It is our conjecture that these optimum values will also work for other FG bodies.

5. Conclusions

It has been shown that for wave propagation in a functionally graded elastic material, the MSPH method gives results very close to those obtained analytically. The artificial viscosity is considered to diminish oscillations near the shock front. Because the material considered is inhomogeneous, the wave speed and the magnitude of the shock front change as the wave propagates in the plate.

By introducing a criterion to determine the error in the computed results, we have examined in detail the effect of the artificial viscosity on the accuracy of the computed solution. It has been shown that a proper value of the linear artificial viscosity can greatly reduce the error, while the quadratic artificial viscosity has a negligible effect. We have also compared results computed by the FE and the MSPH methods. For all values of the linear artificial viscosity coefficient, the MSPH method with the initial smoothing length $h = 1.1$ times the minimum distance, Δ , between any two adjacent particles gives slightly lower error than the FEM. For $h = 1.1\Delta$, the values of the equivalent linear artificial viscosity coefficient at which the relative stress error is minimum are nearly equal for both the FE and the MSPH methods. The optimum value of the linear artificial

viscosity coefficient for the MSPH method is found to be 0.1, which is close to that used in the FEM but much smaller than that used in the SPH method.

Effects of the number of particles, the smoothing length and the kernel function upon the relative error in the computed solution have also been delineated. The error decreases with an increase in the number of particles, and a decrease in the smoothing length. However, for uniformly spaced particles in the uniaxial strain problem, the smoothing length must be greater than the distance between adjacent particles. By comparing results computed with four different kernel functions, it is found that the modified Gauss function gives the smallest value of the error, and is thus recommended for the MSPH method.

Acknowledgments

This work was partially supported by the Office of Naval Research grants N00014-98-1-3000 and N00014-06-1-0567 with Dr. Y.D.S. Rajapakse as the program manager. Views expressed herein are those of authors, and not of the funding agency.

References

- [1] S.G. Lekhnitskii, *Theory of Elasticity of an Anisotropic Body*, Mir, Moscow, 1981.
- [2] R.C. Batra, Finite plane strain deformations of rubberlike materials, *Int. J. Numer. Methods Eng.* 15 (1980) 145–160.
- [3] M. Yamanouchi, M. Koizumi, T. Hirai, I. Shiota, in: M. Yamanouchi, M. Koizumi, T. Hirai, I. Shiota (Eds.), *Proc. First Int. Symp. Functionally Graded Materials*, Sendi, Tokyo 1990.
- [4] T.J.R. Hughes, *The Finite Element Method: Linear Static and Dynamic Finite Element Analysis*, Prentice Hall, 1987.
- [5] R.C. Batra, B.M. Love, Crack propagation due to brittle and ductile failures in microporous thermoelastoviscoplastic functionally graded materials, *Eng. Fract. Mech.* 72 (2005) 1954–1979.
- [6] T.-C. Chiu, F. Erdogan, One-dimensional wave propagation in a functionally graded elastic medium, *J. Sound Vib.* 222 (1999) 453–487.
- [7] G.M. Zhang, R.C. Batra, Modified smoothed particle hydrodynamics method and its application to transient problems, *Comput. Mech.* 34 (2004) 137–146.
- [8] L.B. Lucy, A numerical approach to the testing of the fission hypothesis, *Astron. J.* 82 (1977) 1013–1024.
- [9] R.A. Gingold, J.J. Monaghan, Smoothed particle hydrodynamics: theory and application to non-spherical stars, *Mon. Not. R. Astron. Soc.* 181 (1977) 375–389.
- [10] L.D. Libersky, A.G. Petschek, High strain Lagrangian hydrodynamics: a three-dimensional SPH code for dynamic material response, *J. Comput. Phys.* 109 (1993) 67–75.
- [11] J.K. Chen, J.E. Beraun, C.J. Jih, An improvement for tensile instability in smoothed particle hydrodynamics, *Comput. Mech.* 23 (1999) 279–287.
- [12] J.K. Chen, J.E. Beraun, C.J. Jih, Completeness of corrective smoothed particle method for linear elastodynamics, *Comput. Mech.* 24 (1999) 273–285.
- [13] R.C. Batra, G.M. Zhang, Analysis of adiabatic shear bands in elasto-thermo-viscoplastic materials by modified smoothed-particle hydrodynamics (MSPH) method, *J. Comput. Phys.* 201 (2004) 172–190.
- [14] L.D.G. Sigalotti, H. López, A. Donoso, E. Sira, J. Klapp, A shock-capturing SPH scheme based on adaptive kernel estimation, *J. Comput. Phys.* 212 (2006) 124–149.
- [15] M.H. Santare, P. Thamburaj, G.A. Gazonas, The use of graded finite elements in the study of elastic wave propagation in continuously nonhomogeneous materials, *Int. J. Solids Struct.* 40 (2003) 5621–5634.
- [16] G.R. Liu, X. Han, K.Y. Lam, Stress waves in functionally gradient materials and its use for material characterization, *Compos.: Part B* 30 (1999) 383–394.
- [17] X. Han, G.R. Liu, K.Y. Lam, Transient waves in plates of functionally graded materials, *Int. J. Numer. Methods Eng.* 52 (2001) 851–865.
- [18] A.H. Harker, J.A. Ogilvy, Coherent wave propagation in inhomogeneous materials: a comparison of theoretical models, *Ultrasonics* 29 (1991) 235–244.
- [19] L.F. Qian, R.C. Batra, L.M. Chen, Free and forced vibrations of thick rectangular plates by using higher-order shear and normal deformable plate theory and meshless local Petrov–Galerkin (MLPG) method, *CMES: Comput. Model. Eng. Sci.* 4 (2003) 519–534.
- [20] L.F. Qian, R.C. Batra, L.M. Chen, Static and dynamic deformations of thick functionally graded elastic plate by using higher-order shear and normal deformable plate theory and meshless local Petrov–Galerkin method, *Compos.: part B* 35 (2004) 685–697.
- [21] L.F. Qian, R.C. Batra, L.M. Chen, Analysis of cylindrical bending thermoelastic deformations of functionally graded plates by a meshless local Petrov–Galerkin method, *Comput. Mech.* 33 (2004) 263–273.
- [22] L.F. Qian, R.C. Batra, Transient thermoelastic deformations of a thick functionally graded plate, *J. Therm. Stresses* 27 (2004) 705–740.
- [23] R.C. Batra, J. Jin, Natural frequencies of a functionally graded rectangular plate, *J. Sound Vib.* 282 (2005) 509–516.

- [24] A. Ferreira, R.C. Batra, Natural frequencies of orthotropic, monoclinic and hexagonal plates by a meshless method, *J. Sound Vib.* 285 (2005) 734–742.
- [25] U. Andreaus, R.C. Batra, M. Porfiri, Vibrations of cracked Euler–Bernoulli beams using meshless local Petrov–Galerkin (MLPG) Method, *CMES: Comput. Model. Eng. Sci.* 9 (2005) 111–131.
- [26] A.J.M. Ferreira, R.C. Batra, C.M.C. Roque, L.F. Qian, R.M.N. Jorge, Natural frequencies of functionally graded plates by a meshless method, *Compos. Struct.* 75 (2006) 593–600.
- [27] R.C. Batra, M. Porfiri, D. Spinello, Free and forced vibrations of a segmented bar by a meshless local Petrov–Galerkin (MLPG) formulation, *Comput. Mech.*, doi:10.1007/s00466.006.0049.6.
- [28] LS-DYNA theoretical manual, Livermore Software Technology Corporation, 1998.
- [29] J.J. Monaghan, Smoothed particle hydrodynamics, *Annu. Rev. Astron. Astrophys.* 30 (1992) 543–574.
- [30] T. Rabczuk, J. Eibl, L. Stempniewski, Numerical analysis of high speed concrete fragmentation using a meshfree Lagrangian method, *Eng. Fract. Mech.* 71 (2004) 547–556.
- [31] G.R. Johnson, Artificial viscosity effects for SPH impact computations, *Int. J. Impact Eng.* 18 (1996) 477–488.